Turkish Journal of Electrical Engineering & Computer Sciences

http://journals.tubitak.gov.tr/elektrik/

Research Article

Turk J Elec Eng & Comp Sci
(2019) 27: 1571 – 1588

doi:10.3906/elk-1810-138

Invisible watermarking framework that authenticates and prevents the visualization of anaglyph images for copyright protection

David-Octavio MUÑOZ-RAMIREZ*, **Volodymyr PONOMARYOV**, **Rogelio REYES-REYES**
Clara CRUZ-RAMOS, **Beatriz P. GARCIA-SALGADO**
Superior School of Mechanical and Electrical Engineering (ESIME) Culhuacán, The National Polytechnic Institute, Mexico City, Mexico

Received: 20.10.2018 • **Accepted/Published Online:** 19.02.2019 • **Final Version:** 15.05.2019

Abstract: In this work, a watermarking framework to authenticate and protect the copyright that prevents the visualization of nonauthorized anaglyph images is proposed. Designed scheme embeds a binary watermark and the Blue channel of the anaglyph image into the discrete cosine transform domain of the original image. The proposed method applies the quantization index modulation-dither modulation algorithm and a combination of Bose–Chaudhuri–Hocquenghem with repetition codes, which permit to increase the capability in recovering the watermark. Additionally, Hash algorithm is used to scramble the component where the watermark should be embedding, guaranteeing a higher security performance of the scheme.

This new technique prevents the visualization of 3D content to unauthorized users. Additionally, its high robustness against the most common image processing attacks, such as JPEG compression, impulsive and Gaussian noises, etc. has been demonstrated in this study.

Key words: Invisible watermark, anaglyph, authentication, copyright protection, blind extraction, discrete cosine transform, quantization index modulation-dither modulation, Bose–Chaudhuri–Hocquenghem

1. Introduction

In recent years, the quest for a more realistic 3D experience has increased. Currently, 3D content can be found in DVD, Blu-ray Discs, video games, and virtual reality even printed in magazines and trading cards, permitting a simpler distribution and access to a wider number of people.

Anaglyph viewing methods are known as efficient and low-cost techniques to generate 3D content. Anaglyph images are based on the binocular vision phenomenon, which was patented by Louis Ducos in 1891. Anaglyph images are easily created by the combination of color components, commonly red and cyan [1]. These components are obtained from two images with a distinct point of view. Once the images are blended, the 3D perception can be performed. This kind of images have different areas of application, such as entertainment [2], education, and clinical research [3] among others. However, the easy access and simple generation of anaglyph images has caused many issues, for example, the distribution of illegal copies or the modification by an unauthorized user, which damages the copyright of the images. Consequently, the protection of copyright and content of multimedia files has become remarkably important. To solve this problem, there exist diverse techniques known as watermarking [4] that consists of embedding additional information of the owner in the digital content to be protected [5]. Each watermarking method should satisfy the following requirements:

*Correspondence: dmunozr1302@alumno.ipn.mx

- **Quality:** The quality of the cover file should not be significantly degraded.
- **Robustness:** The watermarked file should be robust enough against intentional or unintentional attacks.
- **Capacity:** The number of bits that the host file can contain should be suitable.

Most of the existing watermarking methods can only satisfy one or two of the above requirements, and not all of them are robust against every attack [6]. Therein lays the importance to develop a good watermarking technique that accomplishes the balance between these three properties. Another point worth mentioning is that depending on the use of the watermarking scheme and its specifications (low computational cost, speed, etc.), the embedding process can be performed in the spatial or frequency domain [6]. On the one hand, the embedding techniques in spatial domain are faster and simpler in comparison with the frequency domain methods. An example of this approach can be observed in the techniques based on least significant bit [7], where the watermark is embedded directly into the pixels of the host images. However, the principal drawback of this technique is the lack of robustness against different image processing attacks. On the other hand, in the watermark techniques applied in the frequency domain transform, for the cover image, a transformation algorithms such as fast Fourier transform [8], discrete cosine transform (DCT), discrete wavelet transform (DWT)[9], or other similar algorithms are used, and usually, the watermark information is embedded into the coefficients of the selected transform.

In this study, we propose a novel scheme for the authentication and copyright protection of anaglyph images (ACAI) based on two-level DCT, third-level DWT, and error correcting codes (ECC). In the designed technique, the color components (R, G, and B) of the anaglyph are separated because the R channel represents one image of the pair-stereo and it is used as the carrier component. In addition, G and B channels, which represent the other stereo pair image, are also disjointed, and G remains unchanged while B is embedded into R channel. In the insertion and extraction process, we employ quantization index modulation-dither modulation (QIM-DM) [10] technique that was proposed by Chen and Wornel, this method is widely used in image [11, 13] and audio watermarking schemes due to their excellent robustness against distortions. Quantization index modulation (QIM) inserts data by modulating a sequence of indexes in combination with the secret information, and then quantifying the cover signal with the quantifier sequence index associated with the secret data. Dither modulation (DM) is a variant that improves the performance of the QIM algorithm. In QIM-DM, a special parameter named "dither vector" is used in the embedding and extraction process of the watermark increasing the robustness of the watermarking scheme against attacks. QIM-DM can be calculated as follows:

$$s'(x;m) = q(x + d(m)) - d(m), \tag{1}$$

where $s'(x;m)$ is the modulated signal, and $q(\cdot)$ is the base quantifier, which depends on original signal x, the watermark m, and the dither vector $d(\cdot)$.

Nonetheless, this method is not capable to correct errors owing to the not utilization of any redundant information. Therefore, we use ECCs to solve this drawback.

Experimental results have demonstrated that the proposed scheme is robust against JPEG compression, impulsive and Gaussian noise, and other common image processing attacks. Besides, the performance of designed scheme has shown superiority in comparison with other anaglyph watermarking techniques studied in this paper, achieving balance between quality, robustness, and capacity.

The rest of the paper is organized as follows: Section 2 presents a review of related works. In Section 3, principal contributions are enumerated. Section 4 presents the watermark embedding and extraction procedures.

Section 5 discusses the experimental results and their comparison with other state-of-art schemes. Finally, Section 6 concludes the paper.

2. Related works

Over the last ten years, several promising watermarking schemes for 3D content have been developed and implemented. There are methods for 3D models [14], 3D meshes [15], deep image-based rendering [16, 18], and stereo images [19, 21]. However, there are not enough studies concerning the protection of anaglyph images since only a few articles have been published in this area.

According to Smolic et al. [22], 3D content can be protected depending on the way the watermark is inserted and extracted (3D/3D, 3D/2D, and 2D/2D).

Deng et al. [23] proposed a 3D/3D method, in which a gray-scale image is decomposed by 2D-DWT and each pixel is quantified individually. Insertion process uses a combination of Nielson norm and the redundancies of the triangle meshes. In the extraction process, the information is recovered according to the order of the vertices of the triangles and the Nielson standards. Experimental results show that the algorithm is resistant to Gaussian noise attacks, obtaining a value of 0.72 for the correlation coefficient (CC), but it does not show information of other type of evaluation criteria.

Alternatively, García and Dugelay [24] proposed a 3D/2D method where the watermark is embedded into the texture of a 3D object, and the watermark is extracted from the recovered texture using the 2D projection of the 3D image. This technique resists up to 75% JPEG compression but fails against noise attacks.

Bhatnagar et al. [25] proposed a 2D/2D watermarking method based on fractional Fourier transform (FrFT) and reversible integer transform (RIT) for embedding a gray-scale image into an anaglyph. RGB channels are transformed into secret color channels. Thereafter, each channel is segmented into nonoverlapped blocks of size $p1 \times p2$, and the singular value decomposition (SVD) is calculated and modified. This solution has demonstrated high robustness against different attacks and a high performance in terms of imperceptibility. Nevertheless, their principal drawback is the usage of the original image to recover the watermark, resulting in a nonblind watermarking scheme.

Prathap and Anitha presented [26] a 2D/2D approach to embed a gray-scale image using medium-frequency subbands of DWT, where these subbands are divided into blocks, and Jacket Matrix is used to modify the diagonal elements in each block. Experimental results have demonstrated better visual imperceptibility and resistance against attacks, but the quantity of information that can be embedded is lower in comparison with other similar schemes.

On the other hand, Wang [27] has compared the performance of two different 2D/2D watermarking techniques: spread spectrum (SS) and adaptive dither modulation (DM), where they use anaglyphs as the host and a binary image as watermark. Among these two techniques, DM demonstrated better results than SS in terms of quality metrics (PSNR and BER). However, the principal drawback of this method is that only binary images can be used as the watermarks resulting in a limitation of the embedding capacity.

Rakesh and Krishna [28] presented a 2D/2D scheme-based on FrFT to embed a random sequence or a digital watermark into one of the pair-stereo image, and then generates the anaglyph. This scheme provides additional security to the watermark; however, this algorithm does not prevent the visualization of 3D content.

Finally, Devi and Singh [29] have proposed a back propagation network (BPN) to find the best DWT coefficients of LH and HL subbands, and to insert the watermark with a genetic algorithm (GA). Moreover, the

binary image was encrypted using advanced encryption standard (AES) to improve the security. The drawback of this method is that it is not clear how it can be applied to any type of anaglyph. Additionally, this framework presents a high computational cost, which is implied in the training phase of an artificial neuronal network. Besides, if the training stage fails in accuracy it would be impossible to recover the watermark. Another disadvantage lies in the capability of exclusively embedding binary images as watermarks. Thus, only a small quantity of information can be added to the original image. As could be seen, all the analyzed schemes embed the watermark in a transform domain, using different transforms and algorithms, achieving some advantages, and offering enough performance. However, the payload is small and the size of the watermark image is limited. In contrast, in designed scheme the payload is better than the state-of-the-art methods, and the embedding of the watermark does not degrade the quality of the cover anaglyph, going unnoticed to HVS. Besides, proposed scheme presents a novel method to prevent the visualization of 3D content, something that state-of-the-art techniques do not have.

After an exhaustive study of the state-of-the-art, we can conclude that the existing schemes only protects the copyright without preventing the visualization of 3D content. Moreover, the watermarks used in state-of-the-art techniques correspond to binary or gray-scale images only. Nevertheless, the proposed scheme has the potential to insert the mentioned kind of images and color ones. Therefore, the designed method introduces and justifies a novel approach to authenticate and protect the copyright of an anaglyph image.

3. Principal contribution

The principal contributions of the proposed framework in the protection of anaglyph images can be summarized as follows:

- **Prevent the visualization of 3D content.** An authentication of the anaglyph image is performed and the visualization of the 3D content to unauthorized users is prevented.
- **Blind extraction process.** The process does not need any additional information such as the original anaglyph or the original watermark to perform the extraction of the watermark that state-of-the-art techniques use.
- **Balance between quality, capacity, and robustness.** The principal challenge of a watermarking system is to find a balance between quality, robustness, and capacity. Therefore, an experimentation process is performed to find optimal parameters that can achieve this balance.
- **High quality of the reconstructed anaglyph.** Redundancy in the color channels is employed to recover the anaglyph image with a high quality.

4. Proposed framework

4.1. Watermark codification

First, a binary image of size $M \times N$ is taken as the watermark (W), and then with the values of each pixel a one-dimensional vector of $m \times n$ elements is formed $(W_v = [W_0, W_1, W_2, ..., W_n])$. The resulting vector W_v is divided into blocks of size k, and each block is coded (W_c) using BCH (15,7,2). Finally, a repetition code is used in such a way that each element of $W_c = [W_{ci}, W_{c1}, W_{c2}, ..., W_{cn}]$ is repeated 3 times $(W_r = [(W_{c1}, W_{c1}, W_{c1}), ..., (W_{cn}, W_{cn}, W_{cn})])$. The combination of BCH and the repetition code increases the error correction capability and the robustness of the watermark against attacks.

4.2. Watermark embedding

Watermark embedding process is illustrated in Figure 1.

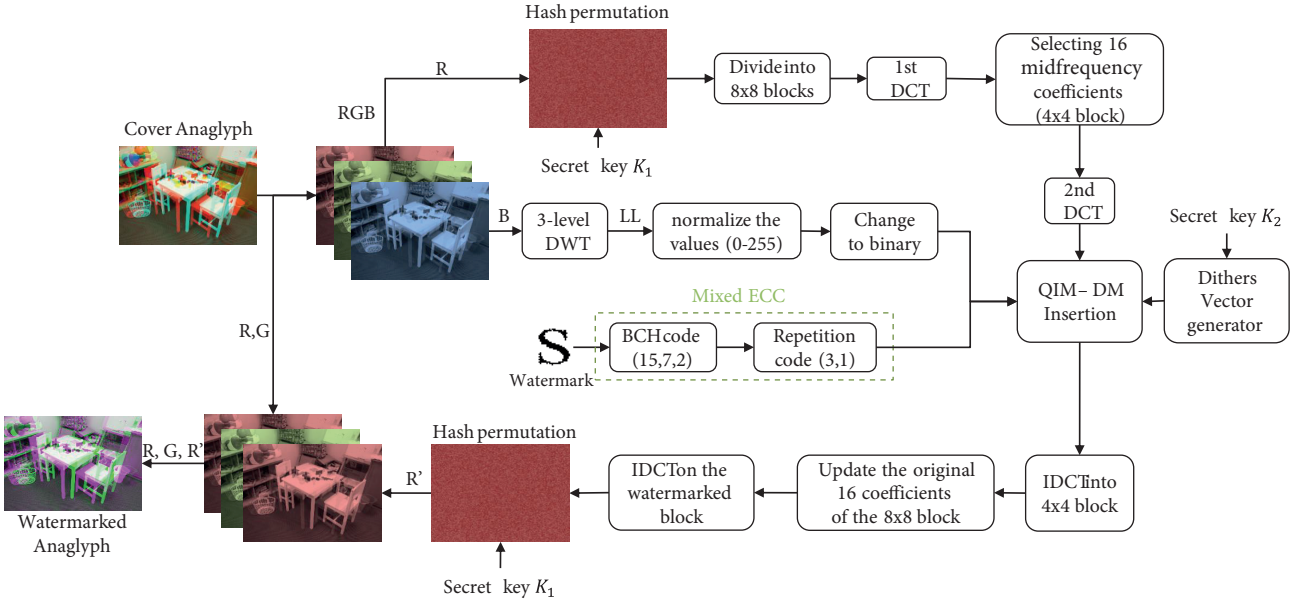

Figure 1. Block diagram of the embedding process (binary image and B channel).

First, the color components of the anaglyph image are separated to only utilize R and B. The R channel is selected to embed the watermark, and it is permuted by Hash algorithm using a secret key K_1.

In the next step, the permuted channel R_p is divided in nonoverlapped blocks of 8×8 pixels and the DCT is applied in each block. After that, the first 16 coefficients of midfrequency are selected (DCT^1_{ac}) and a new matrix of 4×4 coefficients are formed. We used a second DCT in this new matrix, and these new coefficients (DCT^2_{ac}) where the watermark will be embedded.

In the meantime, the B channel is decomposed by DWT until the third level is obtained, and the subband LL^3_B is selected. The values of LL^3_B are normalized. Consequently, all the values follow the constrain $0 \leq LL^3_B \leq 255$.

Afterwards, the 16 coefficients of (DCT^2_{ac}) are used to embed 16 bits of the watermark W_b, this step is repeated until W_b is fully embedded. Both parts are evaluated by QIM-DM as follows:

$$DCT^{2'}_{i,j} = round\left(\frac{DCT^2_{i,j} + d(W_{15i+j})}{\Delta}\right) * (\Delta - d(W_{15i+j})), 0 \leq i \leq M, 0 \leq j \leq 15, 15i + j < T, \quad (2)$$

where $DCT^{2'}_{i,j}$ are the watermarked coefficients of the second DCT, W_{15i+j} stands for watermark bit, $d(W_{15i+j})$ is the dither value corresponding to W_{15i+j}, Δ represents the step-size $(\Delta = 24)$, i and j describe the i^{th} block and the j^{th} position of the block respectively, M is the total blocks of the image, and T denotes the total size of the watermark.

It is important to use two different dither values $(d[k,0]; d[k,1])$ to embed the watermark bits, these values are generated with a random key K_2 and a quantization step-size $\Delta = 24$ using the following equations:

$$d[k,0] = round(\Delta * R) - \Delta, \tag{3}$$

$$d[k,1] = \begin{cases} d[k,0] + \frac{\Delta}{2}, d[k,0] < 0 \\ d[k,0] - \frac{\Delta}{2}, d[k,0] \geq 1 \end{cases} \quad k = 1,2,3,...,16, \tag{4}$$

where R is a random number generator, and the minimum distance between $d[k,0]$ and $d[k,1]$ is $\Delta/2$. These vectors are used to embed the watermark W_{15i+j} bit, depending on their binary value (0, 1).

Each of the resulting blocks $DCT^{2'}_{i,j}$ are returned to the spatial domain via the inverse DCT, and the entire process is repeated until the watermark W_b has been embedded completely.

Finally, R' is permuted again to recover the original pixels positions, and it is joined to the original G and R components, generating the watermarked anaglyph (R', G, R). Table 1 shows the summary of the embedding process.

Table 1. Summary of the insertion algorithm.

for y=1 to AnaglyphHeight/8
for x=1 to Anaglyphwidth/8
for yy=1 to 8
for xx=1 to 8
8x8block(yy,xx) = RHash(yy + posi, xx + posj)
end
end
DCTblock = DCT(8x8block)
k=1;
for i=1 to 4
for j=1 to 4
4x4block(i,j)=DCTblock(apos(k),bpos(k))
k=k+1
end
end
DCT2Nblock=DCT(4x4block)
	for i=1 to 16
	bit=watermark-and-LL-blue-Subband
	randomnumber
	cof=DCT2Nblock(ypos(i),xpos(i))
	Dither = steps×randomnumber - steps;
	if Dither<0
	Dither1=Dither+(steps/2)
	else
	Dither1=Dither-(steps/2)
	end
	if bit=='0'
	dw = round((cof+Dither)/steps)×steps-Dither
	else
	dw = round((cof+Dither1)/steps)×steps-Dither1
	end
	DCT2Nblock(ypos(i),xpos(i))=dw
	end
	IDCT2Nblock=idct2(DCT2Nblock)
		k=1;
		for i=1 to 4
		for j=1 to 4
		4x4blockmarked(apos(k),bpos(k))=IDCT2Nblock(i,j)
		k=k+1
		end
		end
		IDCTblock = idct2(4x4blockmarked)
		for yy=1:8
		for xx=1:8
		RHash(yy + posi, xx + posj)=IDCTblock(yy,xx)
		end
		end
		posj=posj+8;
		end
		posi=posi+8;
		posj=0;
		end

4.3. Watermark extraction

The extraction process of watermark is an inverse procedure of the watermark embedding, as shown in Figure 2.

Firstly, the R' component of the watermarked anaglyph is selected and permuted using a Hash algorithm and secret key K_1 to obtain the pixel positions where the watermark W_b was embedded. Afterwards, R'_p is divided into 8×8 nonoverlapped blocks, and DCT is applied in each one. Subsequently, a second DCT should be performed on the first 16 AC midfrequency values $(DCT^{2'}_c)$.

Eight bits of watermark information (W'_{B_j}) are extracted from each block as follows:

$$W'_{B_j} = \begin{cases} 0 & \text{if } d_{min1} < d_{min2} \\ 1 & \text{otherwised} \end{cases}, \tag{5}$$

where d_{min1} and d_{min2} are calculated by means of the following equations:

$$d_{min1} = \left(round \left(\frac{DCT^{2'}_{i,j} + d[k,0]}{\Delta} \right) * \Delta \right) - d[k,0], \tag{6}$$

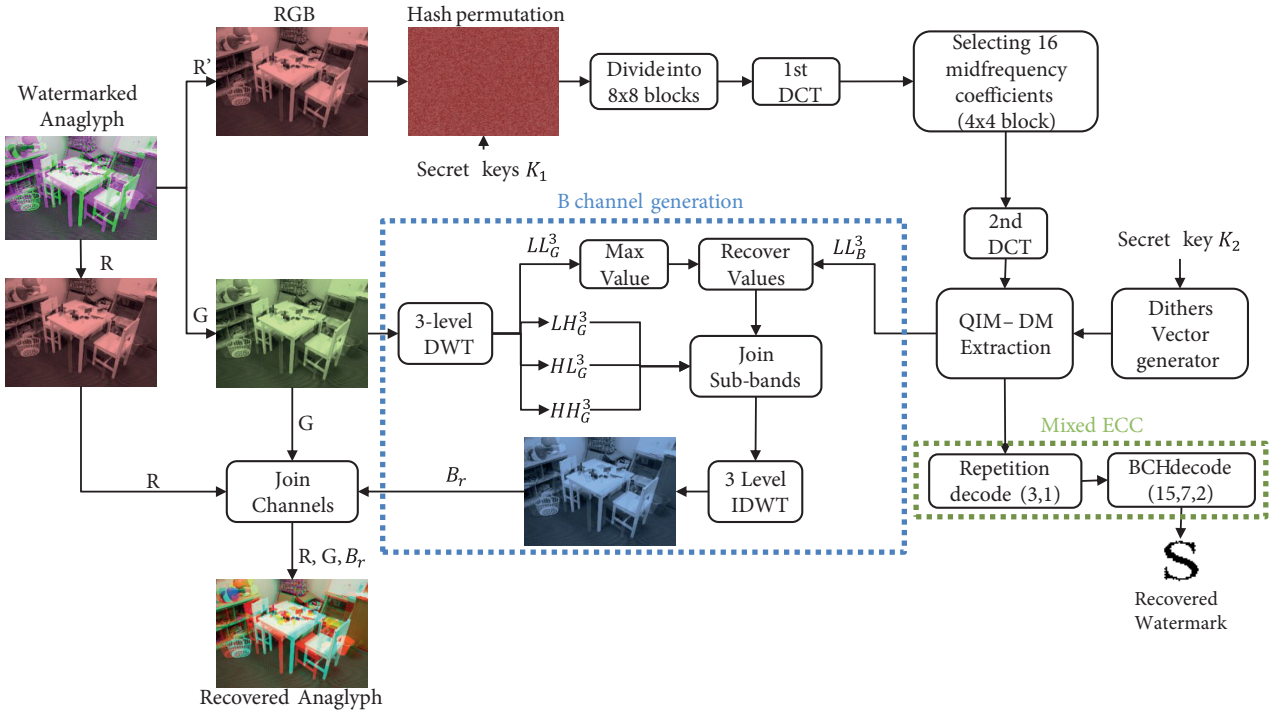

Figure 2. Watermark extraction process (binary image and B channel).

$$d_{min2} = \left(round\left(\frac{DCT_{i,j}^{2'} + d[k,1]}{\Delta} \right) * \Delta \right) - d[k,1], k = 1,2,3,...,16, 0 \leq i \leq M, 0 \leq j \leq 15, \quad (7)$$

where $DCT_{i,j}^{2'}$ is the DCT block, $d[k,0]$ and $d[k,1]$ are two dither values obtained in Eqs. 3 and 4, and Δ is the step-size between $d[k,0]$ and $d[k,1]$, i represents the i^{th} block, j denotes the i^{th} position of the block and M corresponds to the total blocks of the image. These steps should be repeated until W_b' is completely recovered.

Once the binary sequence W_b' is completely recovered, W_b' is divided into two parts, one to generate the subband $LL_B^{3'}$, and the other one to recover the watermark W_r'.

To reconstruct B channel, a third-level DWT is applied to the G channel where the sub-bands LL_G^3, LH_G^3, HL_G^3, HH_G^3 are calculated. These subbands are joined with the recovered subband $LL_B^{3'}$, and IDWT is applied obtaining in B_r.

To recover the watermark, W_r' is transformed to a one-dimension vector of m×n elements ($W_r' = [W_{b1}, W_{b2}, W_{b3}, ..., W_{bn},]$). Thereupon, the vector is divided into $1 \times N$ blocks, where N is the number used in the repetition code. Then, according to majority principle, each element is evaluated and the value that is repeated more times is used to reconstruct the coded signal W_c'. Finally, W_c' are decoded by BCH (15,7,2), resulting in the recovered watermark W'. Table 2 shows only the summary of the extraction process.

4.4. Color watermark potential usage

The proposed method has the ability to employ watermarks represented in exclusively only 8 pure colors: red, green, blue, yellow, cyan, magenta, white, and black. The designed method may binarize these colors in 3 bits,

Table 2. Summary of the extraction algorithm

for y=1 to WatermarkedAnaglyphHeight/8
for x=1 to WatermarkedAnaglyphwidth/8
for yy=1 to 8
for xx=1 to 8
8x8block(yy,xx) = WatermarkedRHash(yy + posi, xx + posj)
end
end
DCTblock = DCT(8x8block)
k=1;
for i=1 to 4
for j=1 to 4
4x4block(i,j)=DCTblock(apos(k),bpos(k))
k=k+1
end
end
	DCT2Nblock=DCT(4x4block)
	for i=1 to 16
	randomnumber
	cof=DCT2Nblock(ypos(i),xpos(i))
	Dither = steps×randomnumber - steps
	if Dither<0
	Dither1=Dither+(steps/2)
	else
	Dither1=Dither-(steps/2)
	end
	S0 = (round(((cof + Dither) / steps))×steps) - Dither
	S1 = (round(((cof + Dither1) / steps))×steps) - Dither1
		$dist_{q1}$ = (cof - S0)^2
		$dist_{q2}$ = (cof - S1)^2
		if ($dist_{q1} \triangleleft dist_{q2}$)
		dw = '0'
		else
		dw = '1'
		end
		recoveredwatermark(index)=dw
		posj=posj+8
		end
		posi=posi+8
		posj=0
		end

and the watermark should be codified considering each set of 3 bits as a color of a pixel. Consequently, more DCT coefficients should be required in the insertion process.

5. Experimental results

The designed framework was implemented in an equipment with Intel® Core i7 (4th Gen) 4500U / 1.8 GHz processor, 8 GB RAM memory and Windows® 10-64 bits. To evaluate the performance of the designed scheme, C# with Microsoft. Net 4.5 framework was used as the platform for such development. In addition, the performance of novel and stae-of-the-art algorithms was evaluated using of pair-stereo images taken from Middleburry Dataset [30]. The following watermark images were used: a binary image of 32×32 pixels and gray-scale images of 50×50 pixels (Figure 3).

Figure 3. Gray-scale and binary watermarks.

Although the proposed framework allows the insertion of color watermarks, the gray-scale and binary images were used for comparison purposes due to the inability of all existing methods to insert color watermarks. The anaglyph images were generated by linear projection algorithm considering red-cyan colors and using images of size 1360×928 pixels: Aloe, Baby, Flowerpot, Lamp shade, Midd1, Doll, Rocks, Wood, Plastic, Monopoly, Adirondack, Bicycle1, Playroom, Playtable, Recycle, Shelves, Sticks, Sword1, Umbrella, and Vintage.

5.1. Quality criteria

To evaluate the effectiveness of the proposed scheme against attacks, the ACAI was evaluated according to the following commonly used objective criteria: Peak signal-to-noise ratio (PSNR), structural similarity index measure (SSIM), and CC.

Criterion PSNR determines how much noise (or artefacts) are added to the anaglyph image after embedding the watermark; using this metric, we can evaluate the quality of the resulting image in an objective way.

Consequently, it can be utilized to calculate the fidelity between the original signal x and the resulting signal y. The results are usually expressed in decibels (dB) as follows:

$$PSNR = 10log_{10}\left[\frac{255^2}{MSE}\right], \tag{8}$$

where MSE is calculated as:

$$MSE = \frac{1}{MN}\sum_{i=1}^{M}\sum_{j=1}^{N}(x(i,j) - y(i,j)), \tag{9}$$

where M and N are the sizes of the image, $x(i,j)$ is the original anaglyph image and $y(i,j)$ is the watermarked anaglyph.

The SSIM is a novel commonly used metric [31] to measure the similarity between two images (x, y) and it is more consistent with the human visual system (HVS) than other previous metrics. Using this quality metric, it is possible to obtain a measure that resembles how the HVS perceives the differences existing in color images, and perceives the characteristics of a color image in terms of luminance l, contrast c, and structure s:

$$SSIM(x,y) = \frac{(2\mu_x\mu_y + c_1)(s\sigma_{xy} + C_2)}{(\mu_x^2\mu_y^2C_1)(\sigma_x^2 + \sigma_y^2 + C_2)}, \tag{10}$$

where x and y are two images to be compared, μ_x and μ_y correspond to the means of x and y; σ_x and σ_y are the standard deviations of x and y, and σ_{xy} represents the correlation coefficient between x and y. The constants C_1, C_2, and C_3 are used to stabilize the algorithm when the denominators approach zero.

CC is a quality metric commonly used to evaluate the robustness of watermark algorithms, and it demonstrates how similar it is to the recovered watermark with respect to the original one, and quantifies the resistance against attacks. The value of ρ between the embedded watermark w and the extracted watermark w' is defined as follows:

$$\rho(w,w') = \frac{\sum_i^n (w_i - \bar{w})(w_i' - \bar{w'})}{\sqrt{\sum_i^n (w_i - \bar{w})^2 (w_i' - \bar{w'})^2}}. \tag{11}$$

A point worth mentioning is that if two watermarks are identical, $\rho = 1$. On the contrary, if they are completely opposite, $\rho = -1$, and if they are completely uncorrelated, $\rho = 0$.

5.2. Parameter selection

The step-size Δ and the combination of ECC codes were experimentally selected according to the better performance of quality criteria. Different anaglyph images that combine detailed regions, edges, and plain areas were used for obtaining better robustness. Among these images, Playroom is a very detailed image with a variety of objects in the background demostrating a lot of edges. Playtable combines different types of textures together with strong edges; finally, Bicycle1 has only smooth areas and a minimum quantity of edges. The rest of anaglyphs images expose a combination of some of the mentioned features.

The proposed scheme was used in each one of the previous anaglyphs utilizing each one of the watermarks presented above yielding average results for comparison. The parameters were changed over a range of values, and the anaglyphs were attacked using JPEG compression, JPEG:2000, impulsive and Gaussian noises.

Obtained PSNR, SSIM, and CC criteria for the proposed scheme have permitted to find the optimal parameter values that give equilibrant balance between quality, robustness, and capacity.

For ACAI, we found that the optimal parameters are given by $\Delta = 24$, BCH (15,7,2) and repetition code (1,3). Figure 4 shows the comparison of the watermarked anaglyphs with the original ones performing no attacks at different values for Δ.

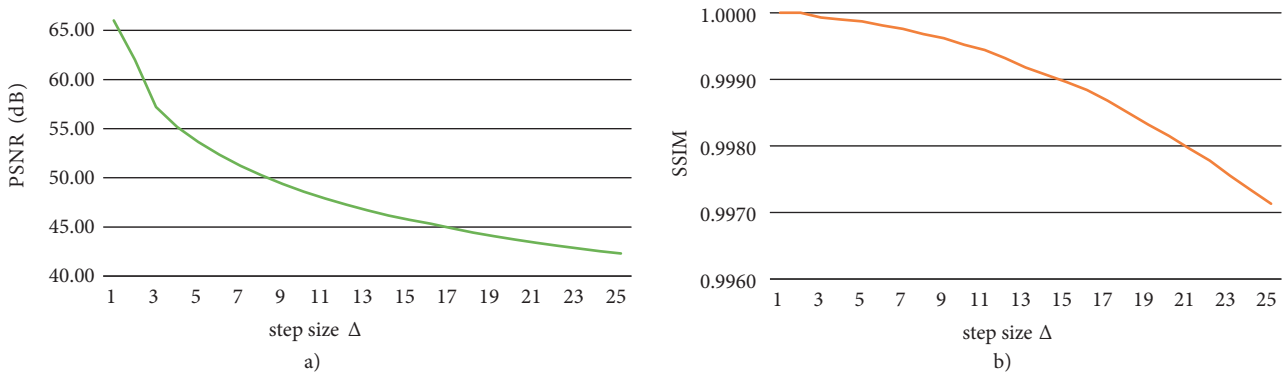

Figure 4. Behavior of average PSNR (a) and SSIM (b) of the watermarked anaglyph images using different Δ values.

The PSNR and SSIM values moderately decrease with the increment of the step Δ, and the quality of the watermarked anaglyph drops. Nonetheless, the reduction of the PSNR and SSIM is still acceptable employing $\Delta = 24$. Table 3 presents the overall performance of the proposed scheme without the use of ECC.

Table 3. Average ρ obtained from the comparison between the original watermarks and the recovered ones for different Δ values.

step-size	$\Delta = 3$	$\Delta = 6$	$\Delta = 9$	$\Delta = 12$	$\Delta = 15$	$\Delta = 18$	$\Delta = 21$	$\Delta = 24$
No attacks	1	1	1	1	1	1	1	1
JPEG QF=75	0.4322	0.6158	0.6777	0.7564	0.7778	0.8136	0.8512	0.8968
JPEG2000 15:1	0.4923	0.5033	0.5463	0.5749	0.5833	0.6637	0.7017	0.7168
Impulsive noise 10%	0.6701	0.6768	0.688	0.6934	0.7325	0.7424	0.7446	0.7354
Gaussian noise $\sigma^2 = 0.005$	0.2265	0.3101	0.4322	0.5185	0.5991	0.7025	0.7957	0.8326
Enlarge 100%	0.7326	0.8239	0.8675	0.8834	0.8917	0.8935	0.8956	0.8972
Reduction 50%	0.7202	0.8115	0.8551	0.871	0.8793	0.8925	0.8975	0.8992
Average filter 3×3	0.1265	0.2101	0.3322	0.4185	0.4991	0.6025	0.6957	0.7326
Median filter 3×3	0.1094	0.1898	0.315	0.3923	0.4874	0.5892	0.6916	0.7637
Brightness adjustment 50%	0.2385	0.3221	0.4442	0.5305	0.6111	0.7145	0.8077	0.8446
Contrast adjustment 50%	0.2395	0.3231	0.4452	0.5315	0.6121	0.7155	0.8087	0.8456

The criterion $\rho = 1$ for all the Δ values when no attacks are performed. Nevertheless, the ρ values present a remarkable reduction when the anaglyph is attacked and the Δ values are small. This behavior is more perceptible in attacks of brightness and contrast adjustment, as well as in average and median filtering. Therefore, given a $\Delta = 24$, the PSNR and SSIM are decreased but a gain in ρ values is obtained when the anaglyph is attacked. Moreover, the CC results are higher than 0.70 for all the attacks selected to prove the performance of the proposed scheme. Consequently, $\Delta = 24$ is selected as the step-size parameter.

In order to select the BCH scheme, seven configurations were selected to find the most robust one to certain attacks. Table 4 shows the overall performance using the selected configuration for BCH and a step-size $\Delta = 24$.

Table 4. Average ρ value from the comparison between the original watermarks and the recovered ones employing different BCH parameters for a step-size $\Delta = 24$.

n	k	t	No attacks	JPEG QF=60	JPEG:2000	Impulsive noise 10 %	Gaussian noise $\sigma^2 = 0.005$	Average filter 3×3
7	4	1	1	0.9173	0.9437	0.9754	0.9763	0.8762
15	11	1	1	0.9032	0.9354	0.9796	0.9751	0.8698
15	7	2	1	1	1	1	1	0.9952
15	5	3	1	1	1	1	1	0.9891
31	26	1	1	0.9362	0.9684	0.9725	0.9887	0.8723
31	21	2	1	0.9992	0.9989	0.9936	0.9985	0.9972
31	16	3	1	1	0.9996	1	0.9954	0.9899

It can be observed that the best results correspond to BCH (15,7,2) and BCH (15,5,3) schemes yielding $\rho = 1$ for the compression and noise attacks and ρ values near 0.99 for the filter attacks. The BCH (15,7,2) has been selected due to its lower redundancy in comparison with BCH (15,5,3). Comparing Tables 3 and 4 in conjunction with Figure 4, it can be observed that the usage of BCH increases the quality of the recovered watermark when $\Delta = 24$, which results in acceptable PSNR and SSIM values, achieving the balance between quality and robustness.

5.3. Imperceptibility testing

When invisible watermarks schemes are used, the imperceptibility of the mentioned watermark should be high, and it should be unnoticed by the HVS. The proposed algorithm was evaluated using all 12 test images. Detailed information of the PSNR and SSIM results for the proposed method is presented in Table 5, where PSNR and SSIM values were above 40 dB and 0.9985, respectively, for all type of anaglyph images and their characteristics. Thus, the high imperceptibility of the watermark in the anaglyph is demonstrated. The comparison of the

Table 5. PSNR and SSIM values of watermarked anaglyphs.

Images	Adirondack	Aloe	Bicycle1	Doll	Flowerpot	Playroom	Playtable	Recycle	Shelves	Sticks	Sword1	Umbrella	Vintage
PSNR (dB)	41.28	41.34	41.52	41.29	41.36	41.31	41.28	41.25	41.29	41.32	41.27	41.29	41.28
SSIM	0.9871	0.9886	0.9895	0.9871	0.9890	0.9884	0.9871	0.9869	0.9881	0.9884	0.9871	0.9872	0.9871

reconstructed anaglyphs and the original ones is performed in terms of PSNR and SSIM (Table 6), where PSNR and SSIM values of the recovered anaglyph are above of 50 dB and 0.998, respectively, demonstrating that novel scheme does not degrade the anaglyph image.

Table 6. PSNR and SSIM values of reconstructed anaglyphs.

Images	Adirondack	Aloe	Bicycle1	Doll	Flowerpot	Playroom	Playtable	Recycle	Shelves	Sticks	Sword1	Umbrella	Vintage
PSNR (dB)	55.54	53.48	52.88	58.52	55.58	56.24	55.94	53.66	55.60	52.65	53.56	57.20	56.55
SSIM	0.9981	0.9972	0.9982	0.9998	0.9988	0.9981	0.9990	0.9972	0.9977	0.9983	0.9977	0.9967	0.9980

5.4. Algorithm complexity

As mentioned in Section 1, the usage of several transforms in watermarking scheme increases the computational cost, but the robustness against attacks can be increased too. Analyzing Table 7, where the computational complexity is exposed, one can observe that the designed algorithm demonstrates this parameter at low level.

Table 7. Algorithmic complexity of ACAI scheme, where height and width represent the size of the anaglyph image, and heightW, as well as widthW, correspond to the sizes of the watermark.

Method	Complexity	Description	Order
Hash permutation	$O(height \times width)$	Each value of the vector with the positions of the pixels is permuted without repetition.	$O(n)$
Divide into 8×8 blocks	$O(height \times width)$	A loop of height $\times$ width is performed in order to divide the image into 8×8 pixel blocks.	$O(n)$
QIM insertion	$O(height \times width)$	16 values are used per each set of 64 pixels. Therefore, 16/64 values of the image are employed.	$O(n)$
DCT	$O(2[height \times width] \log_2 [height \times width])$	DCT is performed with a complexity of (2nlog2n) according to[32, 33]	$O(2n \log_2 n)$
Selecting 16 midfrequency coefficients	$O(16)$	Only 16 values of each 8×8 block are selected.	$O(1)$
3-level DWT	$O(height \times width) + O([height \times width]/4) + O([height \times width]/16) + O([height \times width]/64)$	The first level of decomposition is performed on the whole image; then, the second level is calculated with LL of the previous computation, and the third decomposition is obtained with the LL representation of the second decomposition.	$O(n)$
Change to binary	$O([height \times width]/64)$	The values obtained by means of the third level decomposition of DWT is changed into binary representation.	$O(n)$
$BCH(15, 7, 2)$	$O(height \times width)$	A BCH code is performed on the whole watermark resulting in a major quantity of information.	$O(n)$
Repetition code (3,1)	$O(3 \times 8[(heightW \times widthW)/7])$	Per each pixel a repetition of 3 values is performed. However, as the watermark image is processed by a BCH code, 8 values are added per each set of 7 pixels.	$O(n)$
IDCT	$O(2[height \times width] \log_2 [height \times width])$	The IDCT has the same complexity as DCT.	$O(2n \log_2 n)$
3-level IDWT	$O(height \times width) + O([height \times width]/4) + O([height \times width]/16) + O([height \times width]/64)$	The IWDT has the same complexity as DWT.	$O(n)$
Updating the original 16 coefficients	$O(16)$	The 16 coefficients are ordered. Therefore, the complexity is constant.	$O(1)$

It can be observed that the majority of the methods have an order of $O(n)$ except the DCT and IDCT transforms, which have an $O(2n\log_2 n)$ order. The method uses a total order of $2O(2n\log_2 n) + 8O(n) + 2O(1)$. This means that the higher complexity of the method is in order one corresponding to the transformations resulting that the proposed method needs at least $2O(2n\log_2 n)$ operations. Consequently, the method presents a fair order complexity as its computational time will increase according to the image size; however, the increment is moderately slow.

5.5. Security performance

To increase the security of the proposed scheme, the hash algorithm was used to permute the positions of the pixels inside each component. In this way, the information is embedded along the anaglyph image, and each pixel used for embedding purposes is selected randomly. In addition, the data embedded in each component are independent. Therefore, without the correct secret key, it is impossible to recover the watermark, increasing the safeness of the watermark scheme. Furthermore, this permutation helps the watermark to become unnoticed.

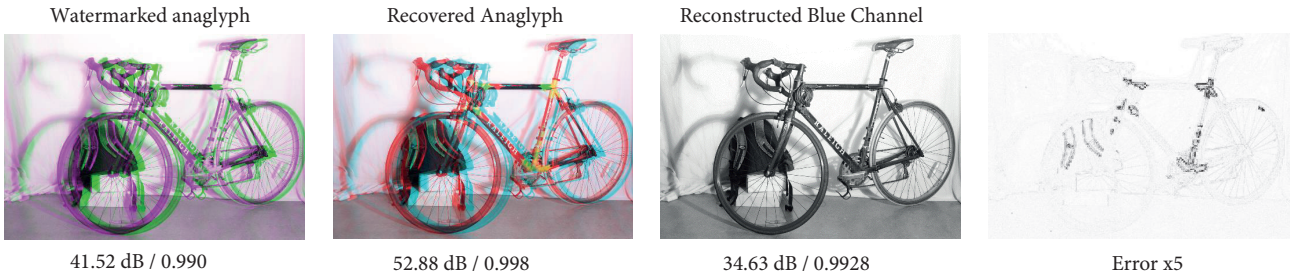

Figure 5. PSNR/SSIM values for Bicycle1 anaglyph.

In addition, the watermarked anaglyphs present a distortion in the color channels in order to avoid the 3D visualization. This distortion can be observed in Figure 5. The watermarked anaglyph needs a reconstruction of the blue channel to allow the 3D visualization because, as it is illustrated in Figure 1, the R' channel is gathered with the R and G channels to compose the watermarked anaglyph. Consequently, B_r component is needed instead of R' to recover the original image. A point worth mentioning is that the secret key K_2 is an imperative requirement to reconstruct B_r. Given these constrains, a high security performance of the proposed scheme is guaranteed.

5.6. Robustness test

It is important that a watermarking system can resist to distinct types of attacks. Robustness represents the strength of the watermark scheme to preserve the watermark image after various intents of eliminating it. Attacks such as JPEG compression, JPEG 2000, impulsive and Gaussian noise degradations, scaling, cropping, brightness and contrast changes were used to test the watermark robustness. After these attacks, the watermarks were recovered, and criterion ρ was calculated. Figure 6 illustrates the behavior of the extracted watermark against to common attacks.

It can be observed in Figure 6 that the designed scheme demonstrates high robustness against JPEG compression since the watermark can be recovered with good quality using a factor QF = 60 or higher due to the resulting value $\rho = 1$, which emphasizes their robustness. For JPEG:2000 test, the watermarked anaglyph was first transformed to this type of image, and then, it was returned to JPEG format, keeping ρ near 1.

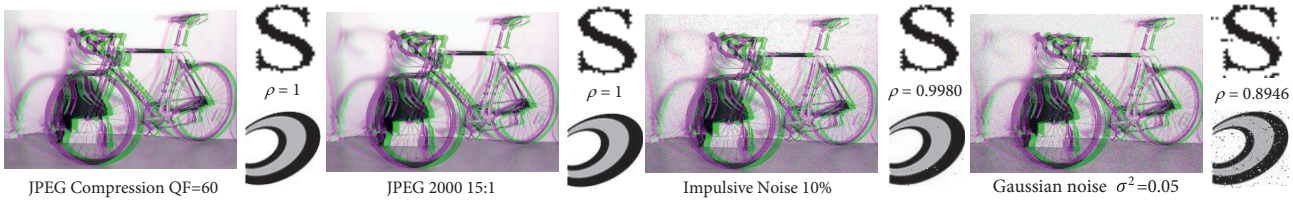

Figure 6. Recovered watermark after the attack to the anaglyph with compression and noise.

The watermark must be capable of surviving the noise degrading of the watermarked anaglyph. When the watermarked image is transmitted via a noisy channel, it can lose information generating additional difficulties in successful recovery of the embedded information. To demonstrate the robustness of the proposed scheme, the watermarked anaglyph has been contaminated with two types of noise. In the first experiment, impulsive noise with 10% intensity has been added, and for the second test, Gaussian noise with $\sigma^2 = 0.05$ has been used for contamination. In both cases, the average criteria values $\rho = 0.9996$ and $\rho = 0.8571$, respectively, have been obtained demonstrating good robustness against these attacks. Furthermore, attacks oriented to size modification, filter application, and brightness and contrast adjustment were performed on the anaglyphs. The resulting ρ values, which compare the recovered watermark to the original, are displayed in Table 8.

Table 8. Criterion ρ for recovered watermark after attack the watermarked anaglyph.

ρ	Adirondack	Aloe	Bicycle1	Doll	Flowerpot	Playroom	Playtable	Recycle	Shelves	Sticks	Sword1
No attacks	1	1	1	1	1	1	1	1	1	1	1
JPEG QF = 60	1	1	1	1	1	1	1	1	1	1	1
JPEG2000 15:1	1	1	1	1	1	1	1	1	1	1	1
Impulsive noise 10%	0.9983	0.9981	0.9984	0.9982	0.9984	0.9985	0.9989	0.9981	0.9985	0.9983	0.9983
Gaussian noise $\sigma^2 = 0.05$	0.8306	0.8429	0.8946	0.8925	0.8937	0.8583	0.8942	0.8499	0.8699	0.8799	0.8852
Enlarge 100%	1	1	1	1	1	1	1	1	1	1	1
Reduction 50%	0.9981	0.9982	0.9982	0.9983	0.9985	0.9981	0.9985	0.9984	0.9982	0.9981	0.9985
Average filter (3 × 3)	0.9918	0.9942	0.9958	0.9921	0.9942	0.9917	0.9898	0.9898	0.9881	0.9941	0.9887
Median filter (3 × 3)	0.9958	0.9954	0.9959	0.9952	0.9932	0.9957	0.9898	0.9928	0.9939	0.9959	0.9943
Brightness adjustment 50%	0.9982	0.9984	0.9989	0.9971	0.9982	0.9987	0.9988	0.9985	0.9982	0.9985	0.9983
Contrast adjustment 50%	0.9982	0.9984	0.9988	0.9971	0.9981	0.9988	0.9987	0.9986	0.9981	0.9987	0.9985

It can be observed that the proposed scheme successfully achieves the recovering of the watermark when compression attacks are used on the anaglyph. According to other attacks, except Gaussian noise, the correlation coefficients result in values over 0.9881, which demonstrates that the watermark can be almost perfectly recovered. The disadvantage of this scheme is observed while Gaussian noise is applied. Nonetheless, the values obtained after this attack are quite acceptable. Consequently, it has been demonstrated that the proposed scheme is robust against ten most common attacks.

5.7. Comparison with other schemes

In order to demonstrate the superior performance of the proposed watermarking scheme against state-of-the-art methods [25, 29], we have evaluated our scheme when the embedded watermark is binary or gray-scale. This limitation is demanded by the mentioned methods because, unlike the designed scheme, they can only use these kinds of watermarks. During this comparison, we use the same images and the same watermarks mentioned above obtaining the following results (see Tables 9 and 10).

Table 9. Comparison of ACAI scheme against state-of-the-art techniques only for the watermark insertion in payload capacity and quality PSNR and SSIM critera.

Method	Watermark	Algorithms	Payload	PSNR	SSIM
Bhatnagar [25]	Gray-scale image	FrFT-RIT-SVD	51200 bits	46.75	0.996
Ivy [26]	Gray-scale image	DWT-Jacket Matrix	51200 bits	53.53	0.999
Wang [27]	Binary image	DCT-SS-DM	2014 bits	47.61	0.997
Rakesh [28]	Binary image	FrFT	1024 bits	43.28	0.993
Hidangmayum [29]	Binary image	DWT-BPN-GA	1024 bits	53.76	0.999
Novel ACAI	Binary or gray-scale image	DCT-DWT-QIMDM-BCH	64731 bits	54.14	0.999

As can be seen in Table 9, the payload of designed ACAI is greater in comparison with the state-of-the-art techniques, since in some cases, the number of bits increases up to 60 times, without affecting the quality of the watermarked anaglyph image, resulting in average, PSNR $>$ 50 dB and SSIM $>$ 0.997.

Table 10. Comparison of quality criterion ρ in recovered watermark using designed ACAI against state-of-the-art techniques.

Attacks	Bhatnagar [25]	Ivy [26]	Wang [27]	Rakesh [28]	Hidangmayum [29]	Novel ACAI
No attacks	1	1	1	1	1	1
JPEG QF=75	0.9746	0.9998	0.9718	N/A	0.9999	1
JPEG2000 15:1	0.7444	0.7859	N/A	N/A	N/A	1
Impulsive noise 10%	0.8572	0.9092	0.9059	0.8416	0.9947	0.9984
Gaussian noise $\sigma^2 = 0.05$	0.7831	0.8253	0.8226	0.8248	0.8271	0.8703
Enlarge 100%	0.9451	0.9708	0.8546	0.9469	0.9998	1
Reduction 50%	0.8674	0.893	0.8435	0.8347	0.9313	0.9945
Average filter (3×3)	0.8489	0.9489	0.9724	0.8436	0.9998	0.9936
Median filter (3×3)	0.9378	0.9915	0.9798	0.8988	0.9998	0.9953
Brightness adjustment 50%	0.9961	0.9989	0.9864	0.9451	1	0.9985
Contrast adjustment 50%	0.9961	0.9989	0.9809	0.9504	0.9998	0.9986

From the performed experiments, we can conclude that the novel framework demonstrates a better performance and robustness against most types of attacks. Our designed scheme performs better than other methods in the case of JPEG compression. Moreover, the compared state-of-the-art techniques are not robust against JPEG:2000 attacks. In addition, the proposed framework presents a better recovering of the watermark given noise injection and size change attacks. Nevertheless, it shows lower but still competitive ρ values in comparison with [29] scheme for filter application as well as brightness and contrast adjustment attacks; besides, the payload is 60 times larger, and the PSNR is competitive. The obtained values indicate that the designed scheme has better or competitive results in most of the cases than the existing methods, and unlike other existing schemes, additionally, this novel framework can prevent the visualization of the 3D content to unauthorized spectators.

6. Conclusions

In this study, an efficient and robust watermarking scheme for anaglyph images has been developed. The proposed method takes advantage of the combination of BCH and repetition code increasing the error correction

capability. Additionally, the permutation of pixels provides a higher degree of security to the scheme. Moreover, the designed scheme is a blind watermarking one, which does not need the original anaglyph or the watermark unlike the other existing techniques. In addition, the main goal of preventing the viewing of 3D content was achieved without deteriorating the anaglyph image. Another point worth mentioning is that a balance between quality, capacity, and robustness is achieved using the selected parameters. Furthermore, experimental results have demonstrated that not only the invisibility of watermarking is guaranteed, but also that it is possible to increase the step-size of Δ to make the scheme more robust against attacks and without damaging the quality of the reconstructed anaglyph. Moreover, in comparison with other methods, it has been proved that the proposed framework has a good performance in the watermark recovering after different types of attacks. Besides, the payload can be increased and it is possible to insert up to 60 times more bits without affecting the quality of the recovered anaglyph image (PSNR $>$ 50 dB and SSIM $>$ 0.997). Finally, the designed scheme can be utilized as a basis for future work involving color watermarks.

Acknowledgment

The authors would like to thank The National Polytechnic Institute (IPN), National Council for Science and Technology (CONACyT, grant 220347), and Commission of Operation and Promotion of Academic Activities (COFAA) of IPN for their support.

References

[1] Zone R. 3-D Revolution: The History of Modern Stereoscopic Cinema. Lexington, KY, USA: University Press of Kentucky, 2012.

[2] Babaei M, Makhzani N, Wong CO, Peng LY. Anaglyph view of kinect 3D stream capture. In: IEEE 2013 International Conference Informatics and Creative Multimedia; Kuala Lumpur, Malaysia; 2013. pp. 110-113.

[3] Rojas GM, Gálvez M, Potler NV, Craddock CR, Margulies DS et al. Stereoscopic three-dimensional visualization applied to multimodal brain images: Clinical applications and a functional connectivity atlas. Frontiers in Neuroscience 2014; 8 (328): 1-14. doi: 10.3389/fnins.2014.00328

[4] Nin J, Ricciardi S. Digital watermarking techniques and security issues in the information and communication society. In: IEEE 2013 27th 2013 27th International Conference on Advanced Information Networking and Applications Workshops; Barcelona, Catalonia, Spain; 2013. pp. 1553-1558.

[5] Khorsnad-Movaghar R, Khaleghi-Bizaki H. A new approach for digital image watermarking to predict optimal blocks using artificial neural networks. Turkish Journal of Electrical Engineering and Computer Sciences 2017; 25: 644-654. doi: 10.3906/elk-1507-232.

[6] Tao H, Chongmin L, Zain JM, Abdalla AN. Robust image watermarking theories and techniques: A review. Journal of Applied Research and Technology 2014; 12(1): 122-138. doi: 10.1016/S1665-6423(14)71612-8

[7] Prashanti G, Sandhyarani K. A new approach for data hiding with LSB steganography. In: Emerging ICT for Bridging the Future - Proceedings of the 49th Annual Convention of the Computer Society of India CSI; Hyderabad, Telangana, India; 2015. pp. 423-430.

[8] Varghese J, Subash S, Bin Hussain O, Nallaperumal K, Ramadan Saady M et al. An improved digital image watermarking scheme using the discrete Fourier transform and singular value decomposition. Turkish Journal of Electrical Engineering and Computer Sciences 2016; 24(5): 3432-3447. doi: 10.3906/elk-1409-12.

[9] Jane O, Elbasi E. A new approach of nonblind watermarking methods based on DWT and SVD via LU decomposition. Turkish Journal of Electrical Engineering and Computer Sciences 2014; 22(5): 1354-1366. doi: 10.3906/elk-1212-75

[10] Chen B, Wornell GW. Quantization index modulation: a class of provably good methods for digital watermarking and information embedding. IEEE Transactions on Information Theory 2001; 47(4): 1423-1443. doi: 10.1109/18.923725

[11] Phadikar A. Multibit quantization index modulation: a high-rate robust data-hiding method. Journal of King Saud University - Computer and Information Sciences 2013; 25(2): 163-171. doi: 10.1016/J.JKSUCI.2012.11.005

[12] Jiang Y, Zhang Y, Pei W, Wang K. Adaptive spread transform QIM watermarking algorithm based on improved perceptual models. AEU - International Journal of Electronics and Communications 2013; 67(8): 690-696. doi: 10.1016/J.AEUE.2013.02.005.

[13] Mitekin V, Fedoseev V. A new QIM-based watermarking algorithm robust against multi-image histogram attack. Procedia Engineering 2017; 201: 453-462. doi: 10.1016/J.PROENG.2017.09.687

[14] An XC, Ni RR, Zhao Y. Visible watermarking for 3D models based on boundary adaptation and mesh subdivision. Journal of Applied Sciences 2016; 34(5): 503-514. doi: 10.3969/j.issn.0255-8297.2016.05.003

[15] Hung-Kuang C, Wei-Sung C. GPU-accelerated blind and robust 3D mesh watermarking by geometry image. Multimedia Tools and Applications 2016; 75(16): 10077-10096. doi: 10.1007/s11042-015-3062-y

[16] Cui C, Niu XM. A robust DIBR 3D image watermarking algorithm based on histogram shape. Journal of the International Measurement Confederation 2016; 92: 130-143. doi: 10.1016/j.measurement.2016.05.079

[17] Cui C, Wang S, Niu X. A novel watermarking for DIBR 3D images with geometric rectification based on feature points. Multimedia Tools and Applications 2017; 76(1): 649-677. doi: 10.1007/s11042-015-3028-0

[18] Al-Haj A, Farfoura ME, Mohammad A. Transform-based watermarking of 3D depth-image-based-rendering images. Journal of the International Measurement Confederation 2017; 95: 405-417. doi: 10.1016/j.measurement.2016.10.016

[19] Yang WC, Chen LH. Reversible DCT-based data hiding in stereo images. Multimedia Tools and Applications 2015; 74(17): 7181-7193. doi: 10.1007/s11042-014-1958-6.

[20] Ou ZH, Chen LH. A robust watermarking method for stereo-pair images based on unmatched block bitmap. Multimedia Tools and Applications 2016; 75(6): 3259-3280. doi: 10.1007/s11042-014-2433-0

[21] Luo T, Jiang G, Yu M, Xu H. Asymmetric self-recovery oriented stereo image watermarking method for three dimensional video system. Multimedia Systems 2016; 22(5): 641-655. doi: 10.1007/s00530-015-0475-4

[22] Smolic A, Mueller K, Stefanoski N, Ostermann J, Gotchev A et al. Coding Algorithms for 3DTV: A survey. IEEE Transactions on Circuits and Systems for Video Technology 2007; 17(11): 1606-1621. doi: 10.1109/TCSVT.2007.909972

[23] Deng H, Zhang J, Chen L, Wang R. A 3D model watermarking algorithm resistant to affine transformation. In: Proceedings - 4th International Conference on Multimedia and Security, MINES; Nanjing, Jiangsu, China; 2012. pp. 549-551.

[24] Garcia E, Dugelay JL. Texture-based watermarking of 3D video objects, IEEE Transactions on Circuits and Systems for Video Technology 2003; 13(8): 853-866. doi: 10.1109/TCSVT.2003.815963

[25] Bhatnagar G, Wu J, Raman B. A robust security framework for 3D images. Journal of Visualization 2011; 14(1): 85-93. doi: 10.1007/s12650-010-0067-5

[26] Prathap I, Anitha R. Robust and blind watermarking scheme for three dimensional anaglyph images. Computers and Electrical Engineering 2014; 40(1): 51-58. doi: 10.1016/j.compeleceng.2013.11.005

[27] Wang C. Robust digital watermarking scheme of anaglyphic 3D for RGB color images. International Journal of Image Processing 2015; 9(3): 156-165.

[28] Rakesh Y, Krishna RS. Digital watermarked anaglyph 3D images using FrFT. International Journal of Emerging Trends & Technology in Computer Science 2015; 41(2): 77-80. doi: 10.14445/22312803/IJCTT-V41P113

[29] Devi HS, Singh KM. A robust and optimized 3D red-cyan anaglyph blind image watermarking in the DWT domain. Contemporary Engineering Sciences 2016; 9: 1575-1589. doi: 10.12988/ces.2016.69156

[30] Scharstein D, Hirschmüller H, Kitajima Y, Krathwohl G, Nešic N et al. High-resolution stereo datasets with subpixel-accurate ground truth. In: German Conference on Pattern Recognition (GCPR), Münster, Germany; 2014. pp. 31-42.

[31] Wang Z, Bovik AC, Sheikh HR, Simoncelli EP. Image quality assessment from error visibility to structural similarity. IEEE Transactions on Image Processing 2004; 13(4): 600-612. doi: 10.1109/TIP.2003.819861

[32] Shao X, Johnson SG. Type-II/III DCT/DST algorithms with reduced number of arithmetic operations. Signal Processing 2008; 88(6): 1553-1564. doi: 10.1016/j.sigpro.2008.01.004

[33] Garcia-Salgado BP, Ponomaryov V, Robles-Gonzalez A, Sadovnychiy S. On the parallel classification system using hyperspectral images for remote sensing applications. In: SPIE Commercial + Scientific Sensing and Imaging, 2018, Orlando, FL, USA; 2018. pp. 10670-10682.